

Compositional dependence of the apatite formation ability of Ti Zr alloys designed for hard tissue reconstruction

著者	Miyazaki Toshiki, Hosokawa Tomoya, Yokoyama Ken'ichi, Shiraishi Takanobu
journal or publication title	Journal of Materials Science: Materials in Medicine
volume	31
page range	110-1-110-8
year	2020-11-09
URL	http://hdl.handle.net/10228/00008523

doi: <https://doi.org/10.1007/s10856-020-06448-9>

[Click here to view linked References](#)

1
2
3
4
5
6
7
8
9
10
11
12
13
14
15
16
17
18
19
20
21
22
23
24
25
26
27
28
29
30
31
32
33
34
35
36
37
38
39
40
41
42
43
44
45
46
47
48
49
50
51
52
53
54
55
56
57
58
59
60
61
62
63
64
65

1 **Compositional dependence of the apatite formation ability of Ti–Zr**
2 **alloys designed for hard tissue reconstruction**

3
4 Toshiki Miyazaki^a, Tomoya Hosokawa^a, Ken’ichi Yokoyama^b, Takanobu Shiraishi^c

5
6 ^aGraduate School of Life Science and System Engineering, Kyushu Institute of
7 Technology, Kitakyushu, Japan

8 ^bDepartment of Materials Science and Engineering, Kyushu Institute of Technology,
9 Kitakyushu, Japan

10 ^cGraduate School of Biomedical Sciences, Nagasaki University, Nagasaki, Japan

11
12 Corresponding author: Toshiki Miyazaki

13 Graduate School of Life Science and Systems Engineering, Kyushu Institute of
14 Technology, 2-4, Hibikino, Wakamatsu-ku, Kitakyushu 808-0196, Japan

15 Tel./Fax: +81-93-695-6025

16 E-mail: tmiya@life.kyutech.ac.jp

1
2
3
4
5
6
7
8
9
10
11
12
13
14
15
16
17
18
19
20
21
22
23
24
25
26
27
28
29
30
31
32
33
34
35
36
37
38
39
40
41
42
43
44
45
46
47
48
49
50
51
52
53
54
55
56
57
58
59
60
61
62
63
64
65

1 **Abstract**

2 Ti–Zr alloys are expected to be novel biomaterials with low stress shielding owing to
3 their lower Young’s moduli than pure Ti. The drawback of metallic biomaterials is that
4 their bone-bonding abilities are relatively low. NaOH and heat treatments have been
5 performed to provide Ti–50Zr with apatite-forming ability in the body environment,
6 which is essential for bone bonding. However, the systematic compositional dependence
7 of apatite formation has not been revealed. In the present study, NaOH treatment of
8 Ti–Zr alloys with various compositions and bone-bonding abilities was assessed in vitro
9 by apatite formation in simulated body fluid (SBF). The corrosion current density in
10 NaOH aqueous solution and the amount of Na incorporated into the surface tended to
11 decrease with increasing Zr content. The apatite-forming ability of the treated alloy
12 significantly decreased when the Zr content was ≥ 60 atom%. This phenomenon is
13 attributed to the (1) low OH content on the surface, (2) low Na incorporation into the
14 treated alloy surface, which enhances apatite formation, and (3) low ability of P
15 adsorption to the Ti–Zr alloy in SBF following Ca adsorption to trigger apatite
16 nucleation. Although the adhesion of the titanate/zirconate layer formed on the surfaces

1
2
3
4
5
6
7
8
9
10
11
12
13
14
15
16
17
18
19
20
21
22
23
24
25
26
27
28
29
30
31
32
33
34
35
36
37
38
39
40
41
42
43
44
45
46
47
48
49
50
51
52
53
54
55
56
57
58
59
60
61
62
63
64
65

1 to the substrates increased as Zr content increased, the adhesion between the apatite and
2 the substrate was still low.

3 **Keywords:** Ti–Zr alloy, NaOH treatment, Apatite, Simulated body fluid, Hard tissue
4 reconstruction

5

6 **Running Heads:** Compositional dependence of the apatite formation ability

7

1
2
3 **1. Introduction**
4
5
6

7 2 Because metallic materials, such as Ti and its alloys, have high mechanical
8
9
10 3 strength and fracture toughness, they are clinically applied to repair hard tissues, such as
11
12
13 4 bone and joints, under high loaded conditions [1]. However, they have the drawback of
14
15
16 5 poor bone-bonding ability leading to low long-term stability of fixation [2]. Formation
17
18
19 6 of bone-like apatite in a body fluid environment is necessary for the material to bond to
20
21
22 7 bone [3]. This type of apatite formation is known to be reproduced even in simulated
23
24
25 8 body fluid (SBF) that mimics the human body fluid composition [4]. Various surface
26
27
28 9 modifications of Ti, such as NaOH treatment [5], hydrogen peroxide treatment [6],
29
30
31 10 anodic oxidation [7], and hydrothermal treatment [8,9], have been proposed to improve
32
33
34 11 the bone-bonding ability of Ti.
35
36
37
38
39
40
41

42 12 Ti–Zr alloys are expected to be novel biomaterials with low stress shielding owing
43
44
45 13 to their lower Young’s moduli than pure Ti. It has mechanical strength comparable to
46
47
48 14 commercialized Ti-29Nb-13Ta-4.6Zr alloy with low Young’s moduli [10,11]. Also,
49
50
51 15 Ti–Zr binary system gives solid solution at any composition [12], therefore the galvanic
52
53
54 16 corrosion in body environment can be suppressed. Shiraishi *et al.* [13] fabricated Ti–Zr
55
56
57
58
59
60
61
62
63
64
65

1 alloys with various compositions and evaluated their mechanical properties, and they
2 found that the Young's modulus decreases to 90 GPa at Ti-60 atom% Zr. It has also
3 been reported that pure Zr [14] and Ti-50 atom% Zr [15,16] subjected to NaOH
4 treatment (and subsequent heat treatment for some metals) shows apatite-forming
5 ability in SBF. However, the systematic compositional dependence of apatite formation
6 has not been reported.

7 In this study, Ti-Zr alloys with different compositions were treated with NaOH
8 aqueous solution, and their apatite-formation abilities were investigated *in vitro* using
9 SBF. The surface structural changes caused by NaOH treatment were analyzed
10 spectroscopically and electrochemically, and their affect on apatite formation was
11 investigated.

12

13 **2. Materials and methods**

14 2.1. Specimen preparation

15 The Ti-Zr alloys, as well as pure Ti and Zr, were prepared by the arc-melting
16 method. NaOH and the reagents used to prepare SBF were purchased from Nacalai

1
2
3 1 Tesque Inc. (Kyoto, Japan). NH_4Cl , ZnCl_2 , NH_3 , and HNO_3 aqueous solutions were
4
5
6
7 2 purchased from FUJIFILM Wako Pure Chemical Co. (Osaka, Japan).
8
9

10 3 The alloy substrates with dimensions of $5 \text{ mm} \times 5 \text{ mm} \times 1 \text{ mm}$ were polished
11
12
13
14 4 with #500 SiC paper. Hereafter, the Ti–Zr alloys containing x atom% Zr are denoted
15
16
17 5 $\text{Ti-}x\text{Zr}$ ($x = 20\text{--}80$). Each substrate was then soaked in 5 mL of 5 M NaOH aqueous
18
19
20
21 6 solution and shaken in a water bath (H-10, Taitec Co., Saitama, Japan) at $60 \text{ }^\circ\text{C}$ and 120
22
23
24 7 strokes/min for 1 day. The substrates were then removed from solution, gently washed
25
26
27
28 8 with ultrapure water, and dried at $60 \text{ }^\circ\text{C}$.
29
30

31 9 32 33 34 35 10 2.2. Soaking in SBF

36
37
38 11 The treated substrates were soaked in 30 mL of SBF containing 142.0 mM Na^+ ,
39
40
41
42 12 5.0 mM K^+ , 2.5 mM Mg^{2+} , 147.8 mM Cl^- , 4.2 mM HCO_3^- , 1.0 mM HPO_4^{2-} , and 0.5
43
44
45 13 mM SO_4^{2-} at $36.5 \text{ }^\circ\text{C}$ for various periods. The pH of the solution was buffered at 7.40
46
47
48
49 14 by 50 mM tris(hydroxymethyl)aminomethane and an appropriate amount of HCl. The
50
51
52
53 15 SBF was prepared according to the literature [4]. After soaking, the substrates were
54
55
56 16 removed from the SBF and then subjected to ultrasonic cleaning with ultrapure water
57
58
59
60
61
62
63
64
65

1
2
3 1 for 30 min to remove excess water-soluble salts on their surfaces.
4
5
6

7 2
8
9
10 3 2.3. Characterization
11
12

13
14 4 The surface structural changes of the substrates were characterized by scanning
15
16
17 5 electron microscopy (SEM, Model S-3500N, Hitachi Co., Tokyo, Japan), energy
18
19
20
21 6 dispersive X-ray spectroscopy (EDX, Model EX-400, Horiba Co., Kyoto, Japan), and
22
23
24 7 thin-film X-ray diffraction (TF-XRD, MXP3V, Mac Science Ltd., Yokohama, Japan). In
25
26
27
28 8 the TF-XRD experiments, CuK α X-ray with voltage and current of 30 kV and 40 mA,
29
30
31
32 9 respectively, was used and the incident beam was fixed at 1° to the surface of each
33
34
35 10 substrate and the scan rate was 0.02°·s⁻¹. In EDX, the atomic ratio of each element was
36
37
38 11 calculated from the peak area in the EDX spectrum by using ZAF correction method.
39
40
41

42 12 Three points were measured for each specimen. Specimens for cross-sectional
43
44
45 13 observation were prepared by embedding in light-curing resin (Technovit 4071, KulZer
46
47
48
49 14 GmbH, Hanau, Germany), cutting and polishing with #80, #120, #240, #500 and #1000
50
51
52 15 SiC paper.

53
54
55
56 16 Rate of corrosion corresponding to surface oxide formation was evaluated by
57
58
59
60
61
62
63
64
65

1 polarization test. It was performed in 1 M NaOH aqueous solution using a potentiostat
2
3
4
5
6
7 (HA-151A, Hokuto Denko Co., Tokyo, Japan) equipped with a saturated calomel
8
9
10 electrode as the reference electrode and a Pt electrode as the counter electrode [17]. The
11
12
13
14 specimens were embedded in acrylic resin and the cross-section was abraded with #120,
15
16
17 #240, and #500 SiC paper. In the polarization test, the sample was first immersed in 1
18
19
20
21 M NaOH aqueous solution for 10 min, and the approximate corrosion potential was
22
23
24
25 measured. The specimens were then polarized from the corrosion potential to the anode
26
27
28 (+1.5 V) or cathode direction (-1.5 V) at a sweep rate of 20 mV min⁻¹. Measurement
29
30
31
32 was performed once for each specimen.

33
34
35 Surface OH formation by NaOH treatment is reported to govern the apatite
36

37
38
39 formation in body environment [5]. Therefore, the concentration of surface OH groups
40
41
42 was determined by formation of a zinc complex [18]. The Zn solution was prepared by
43
44
45
46 mixing 500 mL of 4 M NH₄Cl and 250 mL of 0.4 M ZnCl₂, adjusting the pH to 6.9 with
47
48
49
50 25% NH₃ aqueous solution, and finally adjusting the volume to 1000 mL. Each
51
52
53 specimen was soaked in 150 mL of the Zn solution for 5 min and washed with 150 mL
54
55
56
57 of ultrapure water for 10 min. The washing operation was repeated three times. Each
58
59
60
61
62
63
64
65

1 specimen was then dried for 1 h and soaked in 100 mL of 2.42 M HNO₃ aqueous
2 solution for 10 min. The Zn concentration in the HNO₃ solution was measured by
3 inductively coupled plasma atomic emission spectroscopy (ICPE-9800, Shimadzu Co.,
4 Kyoto, Japan). The surface active OH concentration (C_{OH}) was calculated by the
5 following equation [18]:

$$C_{OH} = \frac{2C_{Zn}VA}{S} \quad (1)$$

6 where C_{Zn} , V , S , and A , are the Zn concentration in the HNO₃ solution (mM), volume of
7 the HNO₃ solution (L), surface area of the specimen (mm²), and Avogadro number (6.02
8 × 10²³), respectively. Measurement was performed three to six times for each specimen.

9
10 The adhesive strength of the apatite layer formed on the specimens was measured
11 by peeling-off test regulated in JIS K 5600. An adhesive tape (CT-15105P, NICHIBAN
12 Co., Ltd., Tokyo, Japan) was attached on the specimens and detached. This operation
13 was repeated 5 times.

14 15 **3. Results**

16 SEM images of the specimen surfaces before and after NaOH treatment are shown

1
2
3 1 in Fig. 1. Before treatment, only polishing scratches were observed in any of the
4
5
6
7 2 specimens. After NaOH treatment, pure Ti and Ti-20Zr showed a network structure
8
9
10 3 composed of flake-like particles of less than 1 μm in size. When the Zr content was 40
11
12
13
14 4 or 50 atom%, formation of a layer without a network structure was observed. Above 50
15
16
17 5 atom% Zr, no layer formed and polishing scratches were observed, similar to before
18
19
20
21 6 treatment.

22
23
24 7 The amounts of OH groups on the specimen surfaces before and after NaOH
25
26
27 8 treatment, which were determined by Zn complex formation method, are shown in Fig.
28
29
30
31
32 9 2. For the untreated specimens, the OH amount was about $1 \times 10^{16} \text{ mm}^{-2}$ irrespective of
33
34
35 10 the Zr content. In contrast, the OH amount on the NaOH-treated Ti specimen was about
36
37
38 11 $4 \times 10^{16} \text{ mm}^{-2}$ and it tended to decrease with increasing Zr content. The OH amount of
39
40
41
42 12 Ti-20Zr was lower than that of Ti and Ti-40Zr. Detailed reason is not clear at present.
43
44
45 13 However, judging from the results that Na content is almost the same and morphology
46
47
48
49 14 of the former was a little different from the latter, difference in OH amount may be
50
51
52 15 attributed to specific surface area. When the Zr content was ≥ 70 atom%, the OH amount
53
54
55
56 16 was almost the same as that of the untreated specimens.
57
58
59
60
61
62
63
64
65

1 The relationship between the Na/(Ti+Zr) ratio on the NaOH-treated specimen
2 surface and the Zr content, which were determined by EDX quantitative analyses, is
3 shown in Figure 3. The Na/(Ti+Zr) ratio was 0.12 for pure Ti. With increasing Zr
4 content, the Na/(Ti+Zr) ratio increased until 40 atom% Zr and then decreased. Na was
5 hardly detected at Zr content ≥ 80 atom%.

6 The relationship between the corrosion current density of the specimen in 1 M
7 NaOH aqueous solution and the Zr content is shown in Figure 4. The corrosion current
8 density monotonically decreased with increasing Zr content, indicating that the
9 corrosion resistance against NaOH increased.

10 The TF-XRD patterns of the untreated and NaOH-treated specimens are shown in
11 Fig. 5. Only the diffraction peaks assigned to the alloys were observed for the untreated
12 specimen. The diffraction angle shifted to lower angle with increasing Zr content. This
13 agrees with the Ti–Zr phase diagram showing an all-proportional solid solution [12].
14 After NaOH treatment, peaks assigned to crystalline zirconium titanate were only
15 observed for Ti–60Zr and Ti–70Zr.

16 SEM-EDX profiles of cross-sections of NaOH-treated specimens. in Fig. 6.

1
2
3 1 Concentration gradient of change Ti and Zr increased with increase in Zr content,
4
5
6
7 2 suggesting that the thickness of the surface oxide layer is decreased.
8
9

10 3 SEM images of the specimen surfaces after NaOH treatment and subsequent
11
12
13
14 4 immersion in SBF for 7 days are shown in Fig. 7. Spherical particles formed on the
15
16
17 5 samples with Zr content ≤ 50 atom%. In the TF-XRD patterns of the specimens shown
18
19
20
21 6 in Fig. 8, broad peaks assigned to poorly crystalline apatite (JCPDS#09-0432) are
22
23
24
25 7 observed at $2\theta = 26^\circ$ and 32° for Zr content ≤ 50 atom%. This means that the formed
26
27
28 8 spherical particles were poorly crystalline apatite.
29
30

31 9 The (Ca or P)/(Ti+Zr) molar ratios of the specimen surfaces with Zr content of
32
33
34
35 10 ≥ 60 atom% after soaking in SBF for 7 days, where no apatite formed, are shown in Fig.
36
37
38
39 11 9. They were determined by EDX quantitative analyses. Both Ca and P were detected
40
41
42 12 for 60 atom% Zr, while only Ca was detected for ≥ 70 atom% Zr.
43
44

45 13 Figure 10 shows SEM images of the specimen surfaces after NaOH treatment and
46
47
48
49 14 subsequent immersion in SBF for 7 days, which were attached and detached with an
50
51
52
53 15 adhesive tape 5 times. Surface titanate/zirconate layer as well as the apatite particles
54
55
56 16 was peeled-off for pure Ti and 20 atom% Zr, while only the apatite particles for 40
57
58
59
60
61
62
63
64
65

1
2
3 1 atom% Zr and 50 atom% Zr.
4
5
6

7 2
8
9
10 3 **4. Discussion**
11
12

13
14 4 The thickness of the surface reaction product significantly decreased at high Zr
15
16
17 5 content (>50 atom% Zr). This is attributed to reduction of the reactivity against NaOH
18
19
20
21 6 aqueous solution. This assumption is supported by the data showing reduction of the
22
23
24
25 7 corrosion current and OH concentration (see Figs. 2 and 4).
26
27

28 8 The surface phases on the alloys produced by NaOH treatment significantly
29
30
31 9 varied depending on the Zr content. The surface phases on the alloys predicted from the
32
33
34
35 10 data in Figs. 2, 3, and 5 are given in Table 1. According to the Pourbaix diagram,
36
37
38 11 HTiO_3^- and HZrO_3^- are stable chemical species around pH 14.7, corresponding to 5 M
39
40
41
42 12 NaOH, meaning that sodium (hydrogen) titanate/zirconate favorably forms [19].
43
44
45
46 13 However, the present result showing no Na incorporation into NaOH-treated Zr is
47
48
49 14 different from that predicted from the Pourbaix diagram (see Fig. 3). It has been
50
51
52
53 15 reported that although Na is observed on the top surface of Zr treated with 6.1 M NaOH
54
55
56 16 at 50 °C by X-ray photoelectron spectroscopy (XPS), it disappears after Ar^+ sputtering
57
58
59
60
61
62
63
64
65

1
2
3 1 for 6 s [20]. Therefore, Na may exist only on the top surface of the present specimens.
4
5

6
7 2 However, from the fact that Zr has a significantly lower corrosion rate than Ti in NaOH
8
9
10 3 solution [20], zirconia hydrogel would be the dominant phase. This is consistent with
11
12
13
14 4 the report by Uchida *et al.* [14], where zirconia hydrogel formed after 20 M NaOH
15
16
17 5 treatment.
18
19
20

21 6 When the Zr content exceeded 50 atom%, the apatite-forming ability significantly
22
23
24 7 decreased (see Figs. 7 and 8). From the result that the specimens formed with the
25
26
27
28 8 zirconium titanate phase did not precipitate apatite, the zirconium titanate phase would
29
30
31 9 not contribute to apatite formation. Ti–OH [21] and Zr–OH [22] groups trigger
32
33
34
35 10 heterogeneous apatite nucleation in the body environment. Therefore, the decrease in
36
37
38
39 11 the OH amount shown in Fig. 2 would suppress apatite formation. In addition, for
40
41
42 12 NaOH-treated Ti, Na⁺ released from the surface sodium titanate is known to increase
43
44
45
46 13 the pH of SBF by ion exchange with H₃O⁺ and the supersaturation degree with respect
47
48
49 14 to apatite, leading to enhancement of apatite formation [5]. In this study, all the
50
51
52 15 specimens showed pH increase by 0.1 to 0.17 after soaking in SBF for 1 day (Data not
53
54
55
56 16 shown). In the case of the alloys with high Zr content, judging from the result that Na is
57
58
59
60
61
62
63
64
65

1
2
3 1 hardly incorporated, pH increase would be attributed to another factor such as
4
5
6
7 2 dissolution of zirconium hydroxide on the surfaces [23]. However, the present results
8
9
10 3 indicate that pH increase do not contribute to the apatite formation at high Zr content.

11
12
13
14 4 Adsorption of P was not observed for the alloys that did not form apatite (see Fig.
15
16
17 5 8). Hanawa and co-workers [24,25] investigated the surface structural changes of the
18
19
20
21 6 surfaces of pure Ti, pure Zr, and Ti–Zr alloys in Hanks’ solution by XPS, and they
22
23
24
25 7 found that pure Zr and Ti–Zr alloys with high Zr content adsorbed P but not Ca.
26
27
28 8 However, such zirconium phosphate was not detected for the present specimens by
29
30
31
32 9 EDX or XRD. This may be because analytical method or chemical state of surface
33
34
35 10 zirconia is different. In addition, zirconia hydrogel produced by the sol–gel method is

36
37
38
39 11 known to have the ability of Ca adsorption [26]. This means that the ion adsorption
40
41
42
43 12 behavior on the passive oxide film on the metal surface and the sol–gel-derived metal
44
45
46
47 13 oxide hydrogel is different, and the adsorption behavior on the surfaces of the present
48
49
50
51
52
53 14 alloys is relatively close to the latter. Apatite nucleation on NaOH- and heat-treated Ti in
54
55
56
57 15 SBF is known to proceed by Ca adsorption followed by P adsorption [27]. It has also
58
59
60
61
62
63 16 been reported that if Ca is adsorbed on zirconia hydrogel in advance, the P adsorption

1
2
3 1 capacity increases [26]. Therefore, the apatite-forming ability may be improved on the
4
5
6
7 2 alloys with high Zr content by appropriate control of the state of Ca adsorption.
8
9

10 3 The surface potential is also an important factor that governs the apatite-forming
11
12
13
14 4 ability. Hashimoto *et al.* [28] investigated apatite formation on Ti metal heat treated in
15
16
17 5 various atmospheres, and they found that a highly negatively (-30 to -15 mV) or
18
19
20
21 6 positively (10 to 15 mV) charged sample tended to form a large amount of apatite. In
22
23
24
25 7 contrast, the Ti–Hf alloy formed with hafnium titanate with a highly negative zeta
26
27
28 8 potential of about -40 mV did not form apatite [29]. This means that the surface charge
29
30
31
32 9 suitable for induction of apatite formation is different depending on the substrate. In
33
34
35 10 future, control of the surface potential should also be investigated.
36
37

38 11 It was found that the adhesion of the titanate/zirconate layer formed on the
39
40
41
42 12 surfaces to the substrates increased as Zr content increased. Considering that the
43
44
45 13 concentration gradient becomes gentle as Zr content increases, it is assumed that the
46
47
48
49 14 stress concentration is suppressed by the formation of the graded structure. However,
50
51
52
53 15 even in the alloys with high Zr content, the adhesion between the apatite and the
54
55
56 16 substrate was low. This is probably because the alloys with high Zr content had a
57
58
59
60
61
62
63
64
65

1 smooth surface after NaOH treatment as shown in Fig. 1, and had little mechanical
2 locking with the apatite. Kim *et al.* reported that heating at 600°C following NaOH
3 treatment is effective for improving the adhesion of surface titanate layer to Ti substrate
4 [30]. However, in this study, the apatite-forming ability was lost for all the specimens
5 after the heat treatment at 600°C (Data not shown). Also, alpha-beta phase transition
6 may occur around 600 to 800°C [12], which deteriorate mechanical properties of the
7 alloys. It is necessary to pursue optimal heat treatment conditions that maintain the
8 apatite-forming ability.

10 5. Conclusions

11 We have found that the apatite-forming ability of NaOH-treated Ti–Zr alloys in
12 SBF is highly dependent on the Zr content. Namely, high Zr content significantly
13 suppresses the apatite-forming ability. This phenomenon is attributed to reduction in the
14 reaction rate in NaOH aqueous solution at high Zr content and the low potential for P to
15 adsorb in SBF. In future, enhancement of the apatite-forming ability of Ti–60Zr is
16 required, because it is has the lowest Young’s modulus among the Ti–Zr alloys.

1
2
3
4
5
6
7
8
9
10
11
12
13
14
15
16
17
18
19
20
21
22
23
24
25
26
27
28
29
30
31
32
33
34
35
36
37
38
39
40
41
42
43
44
45
46
47
48
49
50
51
52
53
54
55
56
57
58
59
60
61
62
63
64
65

1

2 **Acknowledgments**

3 The authors thank Ms. Akiko Nomura and Mr. Kazuo Obara of the Institute for
4 Materials Research, Tohoku University, Sendai, Japan for their assistance with sample
5 alloy preparation. We thank Tim Cooper, PhD, from Edanz Group
6 (www.edanzediting.com/ac) for editing a draft of this manuscript.

7

8 **References**

- 9 1. Breme J, Biehl V. Metallic Biomaterials. Black J, Hastings G, editors. Handbook of
10 Biomaterial Properties, London: Chapman & Hall; 1998:135-213.
- 11 2. Yan WQ, Nakamura T, Kobayashi M, Kim HM, Miyaji F, Kokubo T. Bonding of
12 chemically treated titanium implants to bone. J Biomed Mater Res
13 1997;37:267-275.
- 14 3. Kokubo T, Kim HM, Kawashita M. Novel bioactive materials with different
15 mechanical properties. Biomaterials 2003;24:2161-2175.
- 16 4. Cho SB, Kokubo T, Nakanishi K, Soga N, Ohtsuki C, Nakamura T, Kitsugi T,

1
2
3
4
5
6
7
8
9
10
11
12
13
14
15
16
17
18
19
20
21
22
23
24
25
26
27
28
29
30
31
32
33
34
35
36
37
38
39
40
41
42
43
44
45
46
47
48
49
50
51
52
53
54
55
56
57
58
59
60
61
62
63
64
65

1 Yamamuro. Dependence of Apatite Formation on Silica Gel on Its Structure: Effect
2 of Heat Treatment. J Am Ceram Soc 1995;78:1769-1774.

3 5. Kim HM, Miyaji F, Kokubo T, Nakamura T. Preparation of bioactive Ti and its
4 alloys via simple chemical surface treatment. J Biomed Mater Res
5 1996;32:409-417.

6 6. Wang XX, Hayakawa S, Tsuru K, Osaka A. A comparative study of in vitro apatite
7 deposition on heat-, H₂O₂-, and NaOH-treated titanium surfaces. J Biomed Mater
8 Res 2001;54:172-178.

9 7. Yang BC, Uchida M, Kim HM, Zhang Z, Kokubo T. Preparation of bioactive
10 titanium metal via anodic oxidation treatment. Biomaterials 2004;25:1003–1010.

11 8. Nakagawa M, Zhang L, Udoh K, Matsuya S, Ishikawa K. Effects of hydrothermal
12 treatment with CaCl₂ solution on surface property and cell response of titanium
13 implants. J Mater Sci Mater Med 2005;16:985–991.

14 9. Kawashita M, Matsui N, Miyazaki T, Kanetaka H. Effect of autoclave and hot
15 water treatments on surface structure and in vitro apatite-forming ability of NaOH-
16 and heat-treated bioactive titanium metal. Mater Trans 2013;54:811–816.

1
2
3
4
5
6
7
8
9
10
11
12
13
14
15
16
17
18
19
20
21
22
23
24
25
26
27
28
29
30
31
32
33
34
35
36
37
38
39
40
41
42
43
44
45
46
47
48
49
50
51
52
53
54
55
56
57
58
59
60
61
62
63
64
65

10. Niinomi M. Recent research and development in titanium alloys for biomedical applications and healthcare goods. *Sci Tech Adv Mater* 2003;4:445–454.

11. Ho WF, Chen WK, Wu SC, Hsu HC. Structure, mechanical properties, and grindability of dental Ti-Zr alloys. *J Mater Sci Mater Med* 2008;19:3179-3186.

12. Hari Kumar KC, Wollants P, Delacy L. Thermodynamic assessment of the Ti-Zr system and calculation of the Nb-Ti-Zr phase diagram. *J Alloys Compd* 1994;206:121-127.

13. Shiraishi T, Yubuta K, Shishido T, Shinozaki N. Elastic properties of as-solidified Ti-Zr binary alloys for biomedical applications. *Mater Trans* 2016;57:1986-1992.

14. Uchida M, Kim HM, Miyaji F, Kokubo T, Nakamura T. Apatite formation on zirconium metal treated with aqueous NaOH. *Biomaterials* 2002;23:313-317.

15. Chen X, Nouri A, Lin YJ, Hodgson PD, Wen C. Effect of surface roughness of Ti, Zr, and TiZr on apatite precipitation from simulated body fluid. *Biotech Bioeng* 2008;101:378–387.

16. Chen X, Li Y, Hodgson PD, Wen C. In vitro behavior of human osteoblast-like cells (SaOS2) cultured on surface modified titanium and titanium–zirconium alloy.

1
2
3
4
5
6
7
8
9
10
11
12
13
14
15
16
17
18
19
20
21
22
23
24
25
26
27
28
29
30
31
32
33
34
35
36
37
38
39
40
41
42
43
44
45
46
47
48
49
50
51
52
53
54
55
56
57
58
59
60
61
62
63
64
65

1 Mater Sci Eng C 2011;31:1545-1552.

2 17. Miyazaki T, Sasaki T, Shirosaki Y, Yokoyama K, Kawashita M. Effect of
3 metallographic structure and machining process on the apatite-forming ability of
4 sodium hydroxide- and heat-treated titanium. Bio-Med Mater Eng
5 2018;29:109–118.

6 18. Sakamoto H, Hirohashi Y, Saito H, Doi H, Tsutsumi Y, Suzuki Y, Noda K, Hanawa
7 T. Effect of active hydroxyl groups on the interfacial bond strength of titanium with
8 segmented polyurethane through γ -mercapto propyl trimethoxysilane. Dent Mater J
9 2008;27:81-92.

10 19. Pourbaix M. Atlas of Electrochemical Equilibria in Aqueous Solutions. Houston:
11 National Association of Corrosion Engineers; 1974.

12 20. Motooka T, Yamamoto M. Corrosion behavior of Zr, Ti, Ta and Nb in sodium
13 hydroxide solutions. Zairyo-to-Kankyo 2011;60:394-401 (in Japanese).

14 21. Li P, Ohtsuki C, Kokubo T, Nakanishi K, Soga N, de Groot K. The role of hydrated
15 silica, titania, and alumina in inducing apatite on implants. J Biomed Mater Res
16 1994;28:7-15.

1
2
3
4
5
6
7
8
9
10
11
12
13
14
15
16
17
18
19
20
21
22
23
24
25
26
27
28
29
30
31
32
33
34
35
36
37
38
39
40
41
42
43
44
45
46
47
48
49
50
51
52
53
54
55
56
57
58
59
60
61
62
63
64
65

1 22. Uchida M, Kim HM, Kokubo T, Miyaji F, Nakamura T. Bonelike apatite formation
2 induced on zirconia gel in a simulated body fluid and its modified solutions. J Am
3 Ceram Soc 2001;84:2041-2044.

4 23. Kobayashi T, Sasaki T, Takagi I, Moriyama H. Solubility of zirconium (IV) hydrous
5 oxides, J Nucl Sci Tech 2007;44:90-94.

6 24. Hanawa T, Okuno O, Hamanaka H. Compositional change in surface of Ti-Zr
7 alloys in artificial bioliquid. J Jpn Inst Metals 1992;56:1168-1173 (in Japanese).

8 25. Tsutsumi Y, Nishimura D, Doi H, Nomura N, Hanawa T. Difference in surface
9 reactions between titanium and zirconium in Hanks' solution to elucidate
10 mechanism of calcium phosphate formation on titanium using XPS and cathodic
11 polarization. Mater Sci Eng C 2009;29:1702-1708.

12 26. J. Lin, Y. Zhan, H. Wang, M. Chu, C. Wang, Y. He, X. Wang, Effect of calcium ion
13 on phosphate adsorption onto hydrous zirconium oxide, Chem. Eng. J. 309 (2017)
14 118-129. DOI: 10.1016/j.cej.2016.10.001

15 27. Takadama H, Kim HM, Kokubo T, Nakamura T. An X-ray photoelectron
16 spectroscopy study of the process of apatite formation on bioactive titanium metal.

1
2
3
4
5
6
7
8
9
10
11
12
13
14
15
16
17
18
19
20
21
22
23
24
25
26
27
28
29
30
31
32
33
34
35
36
37
38
39
40
41
42
43
44
45
46
47
48
49
50
51
52
53
54
55
56
57
58
59
60
61
62
63
64
65

1 J Biomed Mater Res 2001;55:185-193.

2 28. Hashimoto M, Ogawa T, Kitaoka S, Muto S, Furuya M, Kanetaka H, Abe M,
3 Yamashita H. Control of surface potential and hydroxyapatite formation on TiO₂
4 scales containing nitrogen-related defects. Acta Mater 2018;155:379-385.

5 29. Miyazaki T, Sueoka M, Shirotsaki Y, Shinozaki N, Shiraishi T. Development of
6 hafnium metal and titanium-hafnium alloys having apatite-forming ability by
7 chemical surface modification. J Biomed Mater Res Part B Appl Biomater
8 2018;106B:2519–2523.

9 30. Kim HM, Miyaji F, Kokubo T, Nakamura T. Effect of heat treatment on
10 apatite-forming ability of Ti metal induced by alkali treatment. J Mater Sci Mater
11 Med 1997;8:341–347.

Table 1 Predicted surface phases formed on the alloys by NaOH treatment

Zr content in atom%	Surface phase
0	Sodium titanate hydrogel
20, 40	Sodium titanate/zirconate hydrogel
60	Sodium titanate/zirconate hydrogel, Crystalline ZrTiO ₄
70	Zirconia/titania hydrogel, Crystalline ZrTiO ₄
80	Zirconia/titania hydrogel
100	Zirconia hydrogel

1
2
3
4
5
6
7
8
9
10
11
12
13
14
15
16
17
18
19
20
21
22
23
24
25
26
27
28
29
30
31
32
33
34
35
36
37
38
39
40
41
42
43
44
45
46
47
48
49
50
51
52
53
54
55
56
57
58
59
60
61
62
63
64
65

1 **Figure captions**

2 **Figure 1** SEM images of the specimen surfaces before and after NaOH treatment.

3 **Figure 2** Relationships between the amounts of OH groups on the specimen surfaces
4 before and after NaOH treatment and the Zr content, which were determined by Zn
5 complex formation method (n=3 for untreated sample and n=6 for treated sample).

6 **Figure 3** Relationship between the Na/(Ti+Zr) molar ratio on the NaOH-treated
7 specimen surface and the Zr content, which was determined by EDX quantitative
8 analyses (n=3).

9 **Figure 4** Relationship between the corrosion current density of the specimen in 1 M
10 NaOH aqueous solution and the Zr content (n=1).

11 **Figure 5** TF-XRD patterns of the untreated and NaOH-treated specimens.

12 **Figure 6** SEM-EDX profiles of cross-sections of NaOH-treated specimens.

13 **Figure 7** SEM images of the specimen surfaces after NaOH treatment and subsequent
14 immersion in SBF for 7 days.

15 **Figure 8** TF-XRD patterns of the specimen surfaces after NaOH treatment and
16 subsequent immersion in SBF for 7 days.

1
2
3
4
5
6
7
8
9
10
11
12
13
14
15
16
17
18
19
20
21
22
23
24
25
26
27
28
29
30
31
32
33
34
35
36
37
38
39
40
41
42
43
44
45
46
47
48
49
50
51
52
53
54
55
56
57
58
59
60
61
62
63
64
65

1 **Figure 9** (Ca or P)/(Ti+Zr) molar ratios of the specimen surfaces with Zr content of
2 ≥ 60 atom% after soaking in SBF for 7 days, which were determined by EDX
3 quantitative analyses (n=3).

4 **Figure 10** SEM images of the specimen surfaces after NaOH treatment and
5 subsequent immersion in SBF for 7 days, which were attached and detached with an
6 adhesive tape 5 times.

Before NaOH treatment

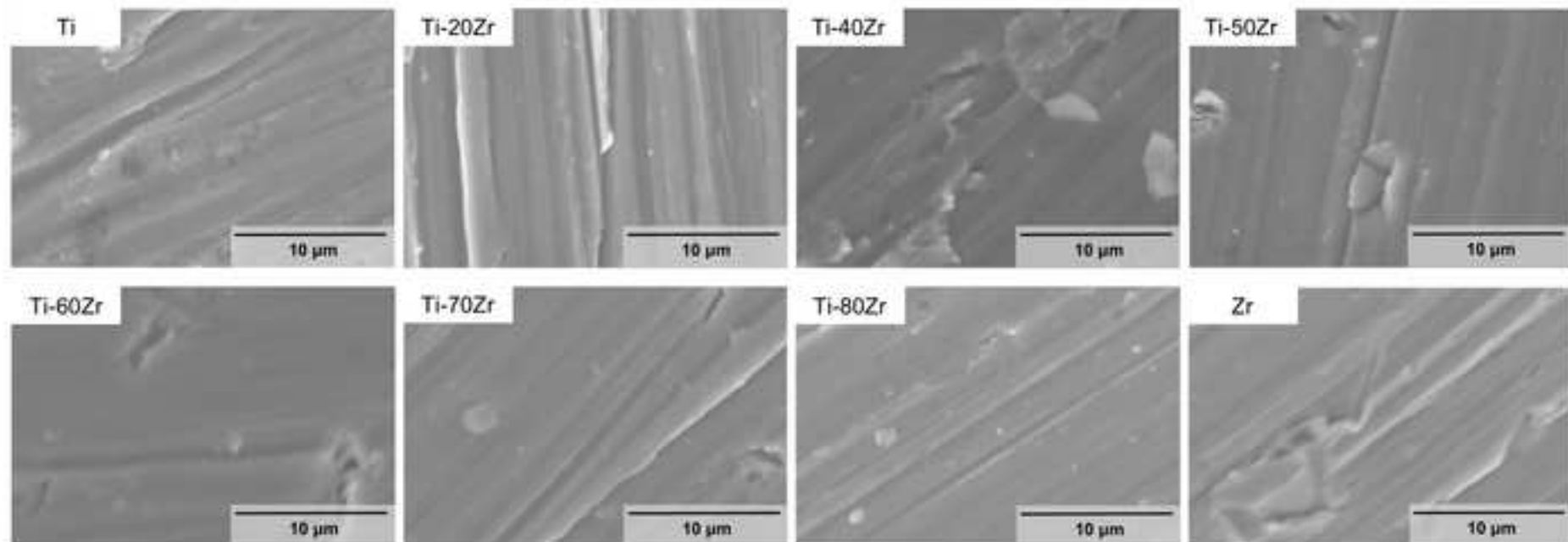


Fig. 1

After NaOH treatment

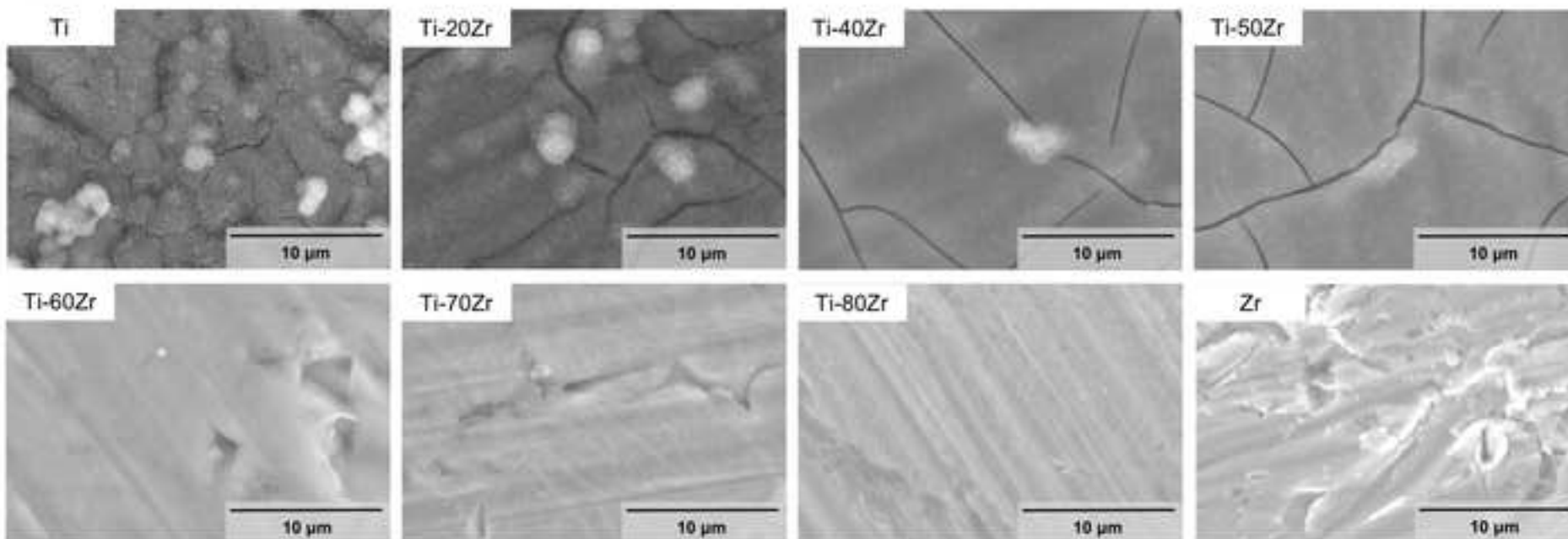


Fig. 1 (Continued)

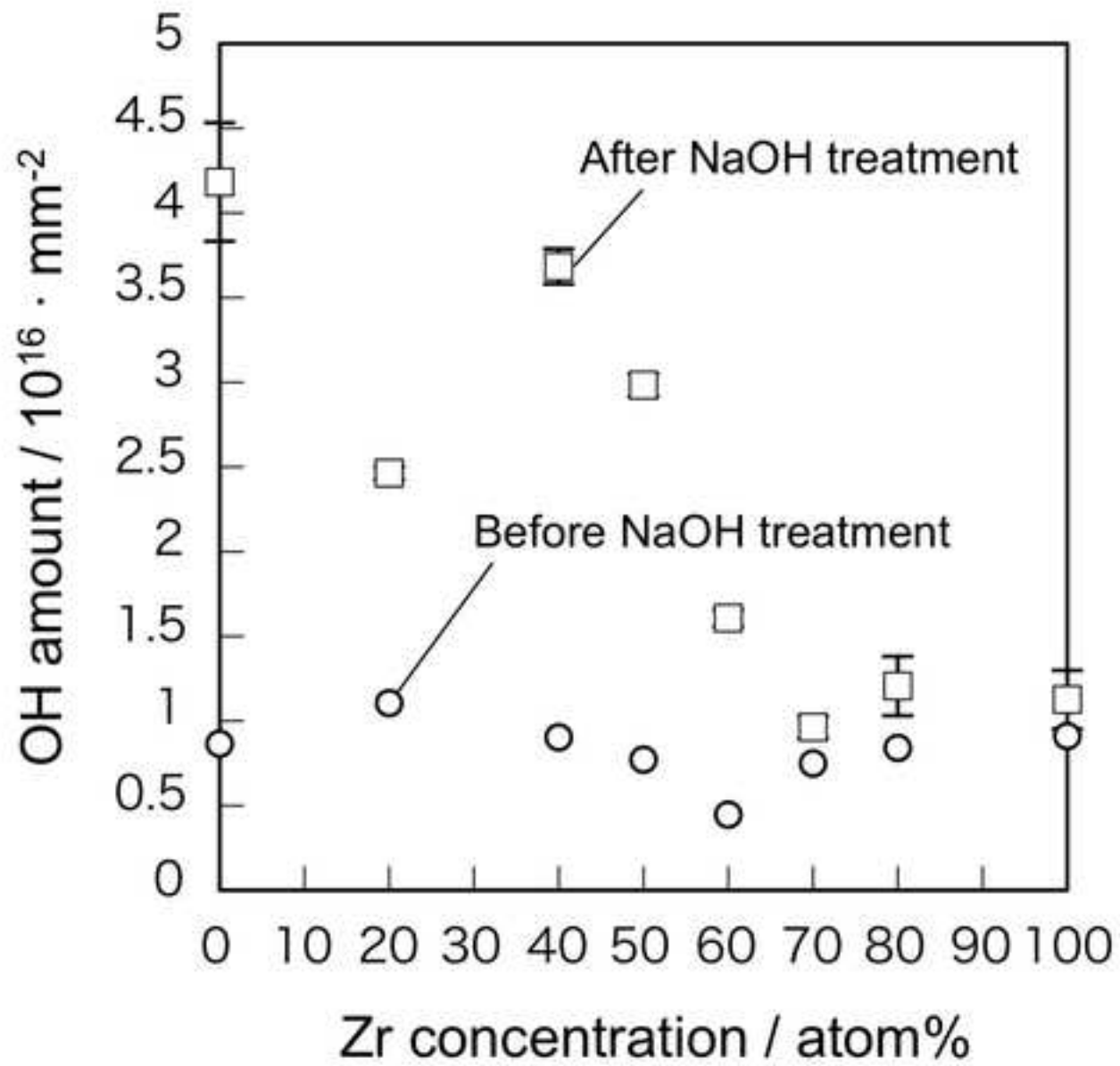


Fig. 2

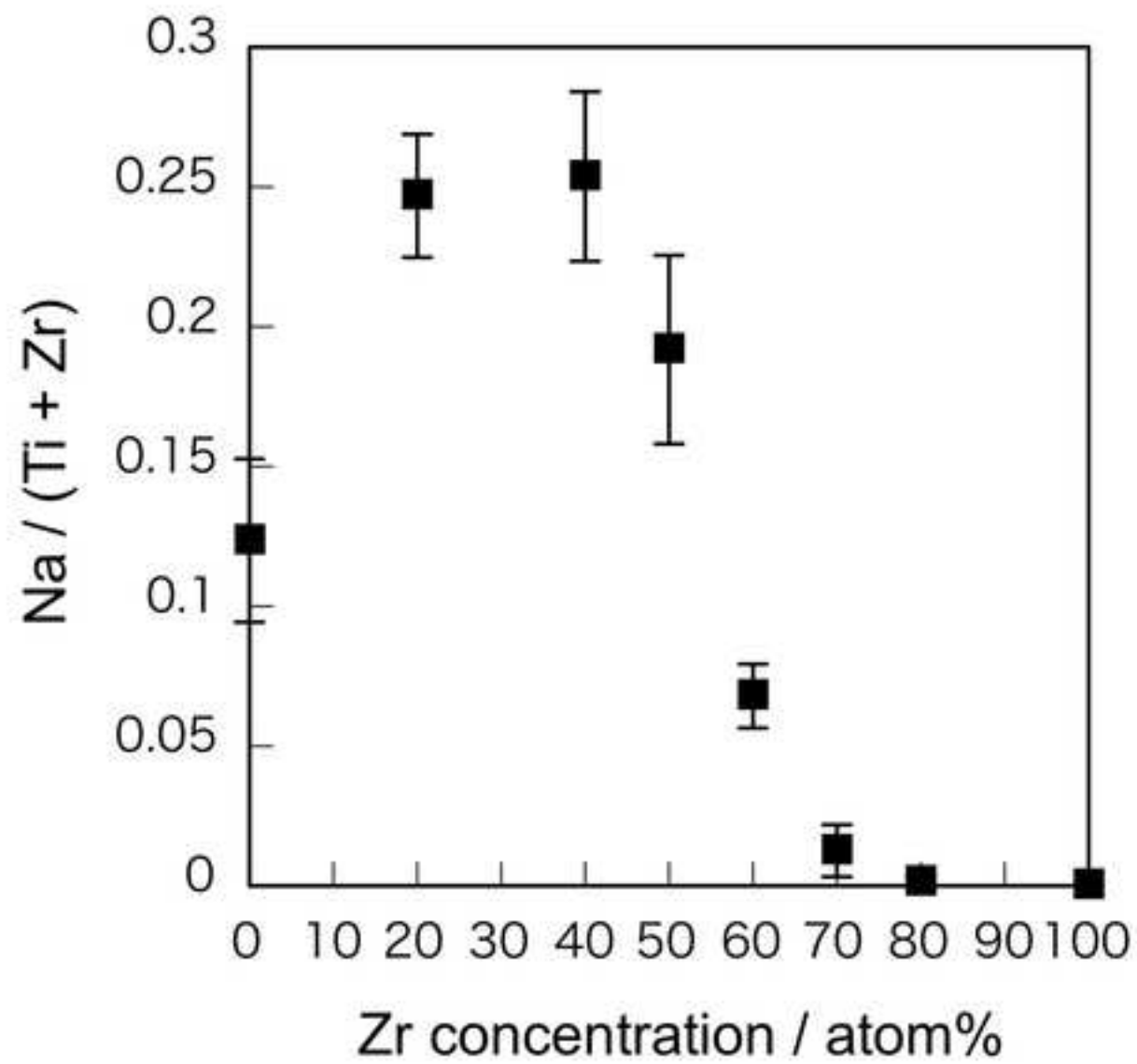


Fig. 3

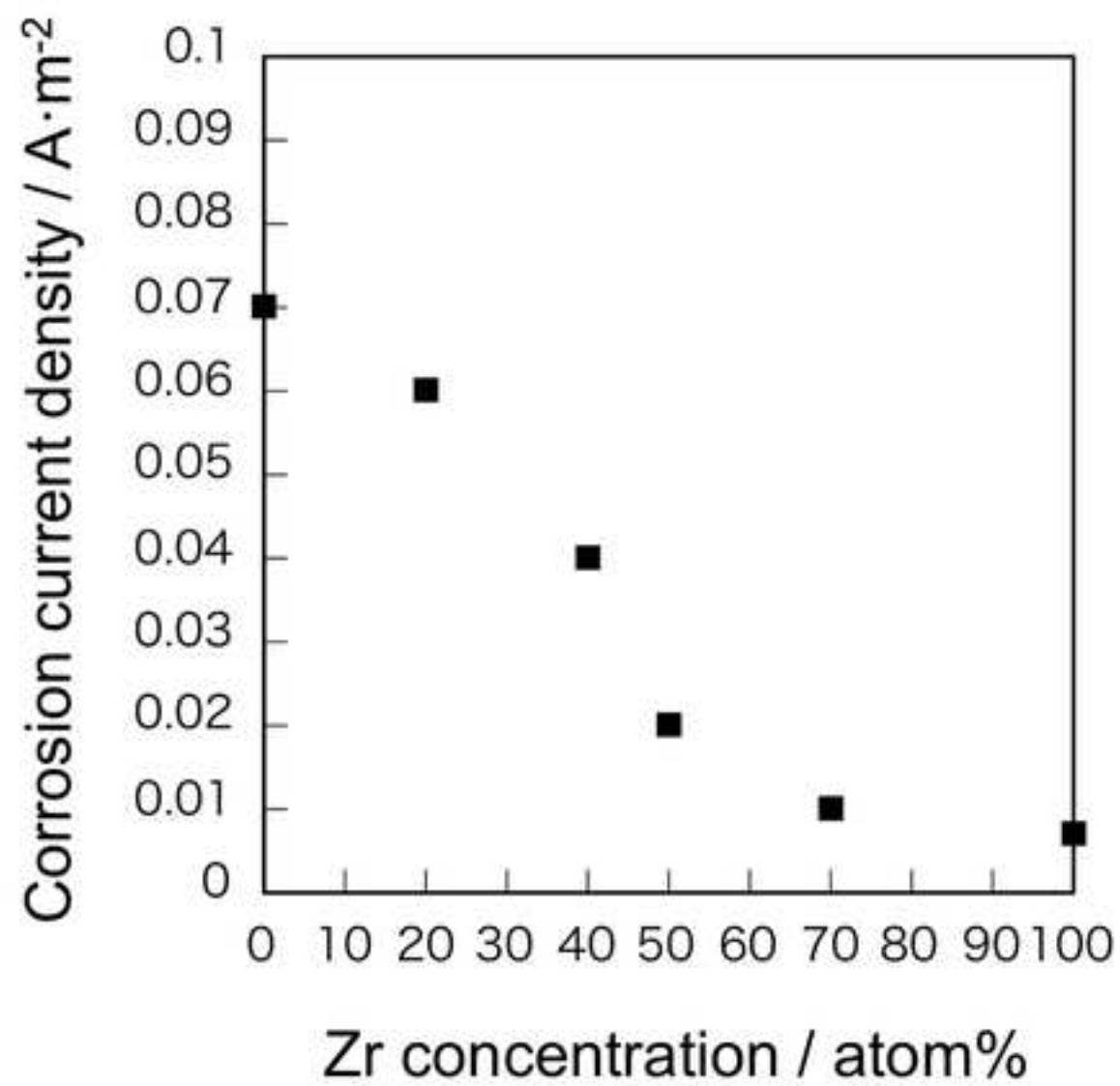


Fig. 4

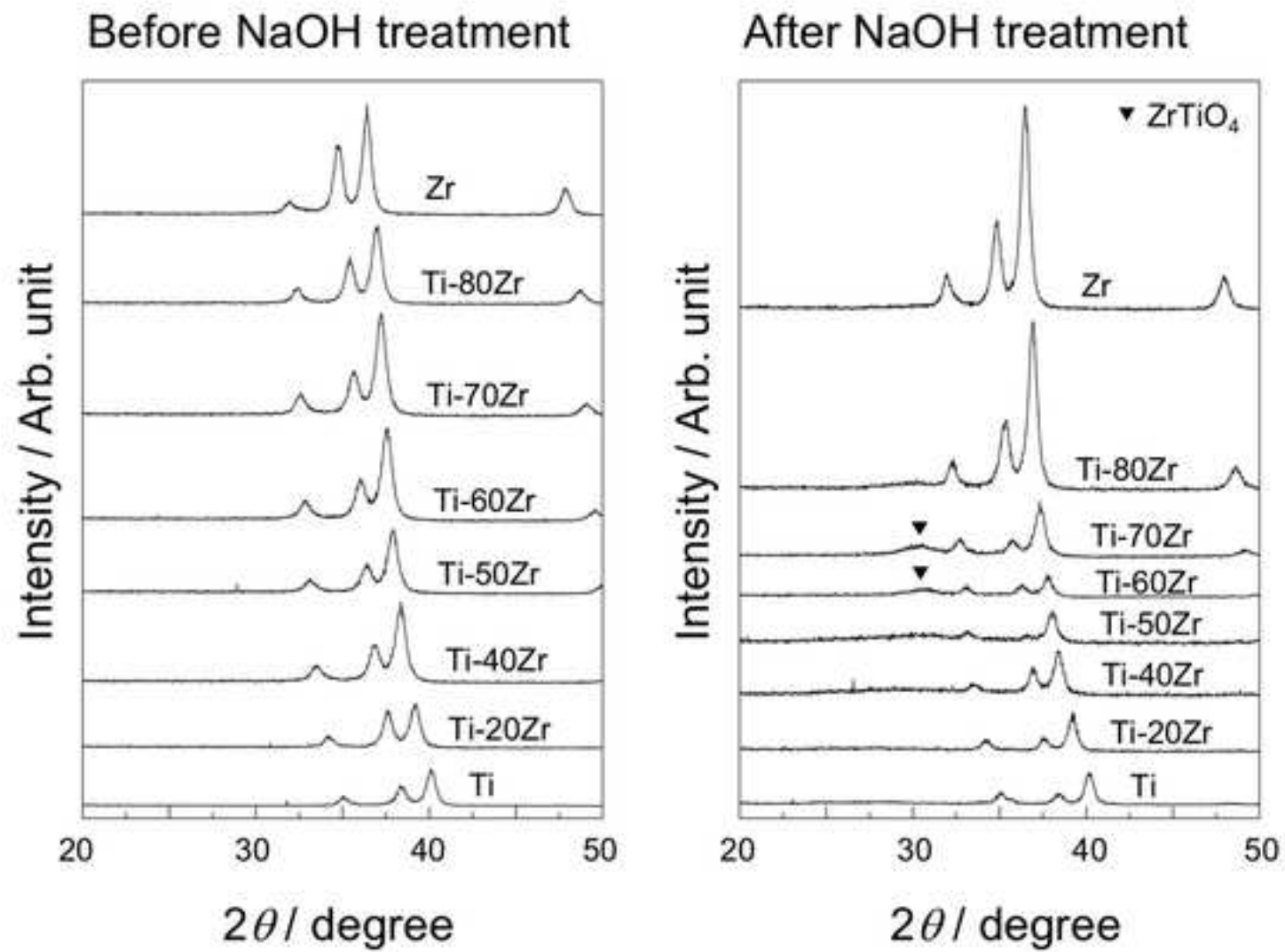


Fig. 5

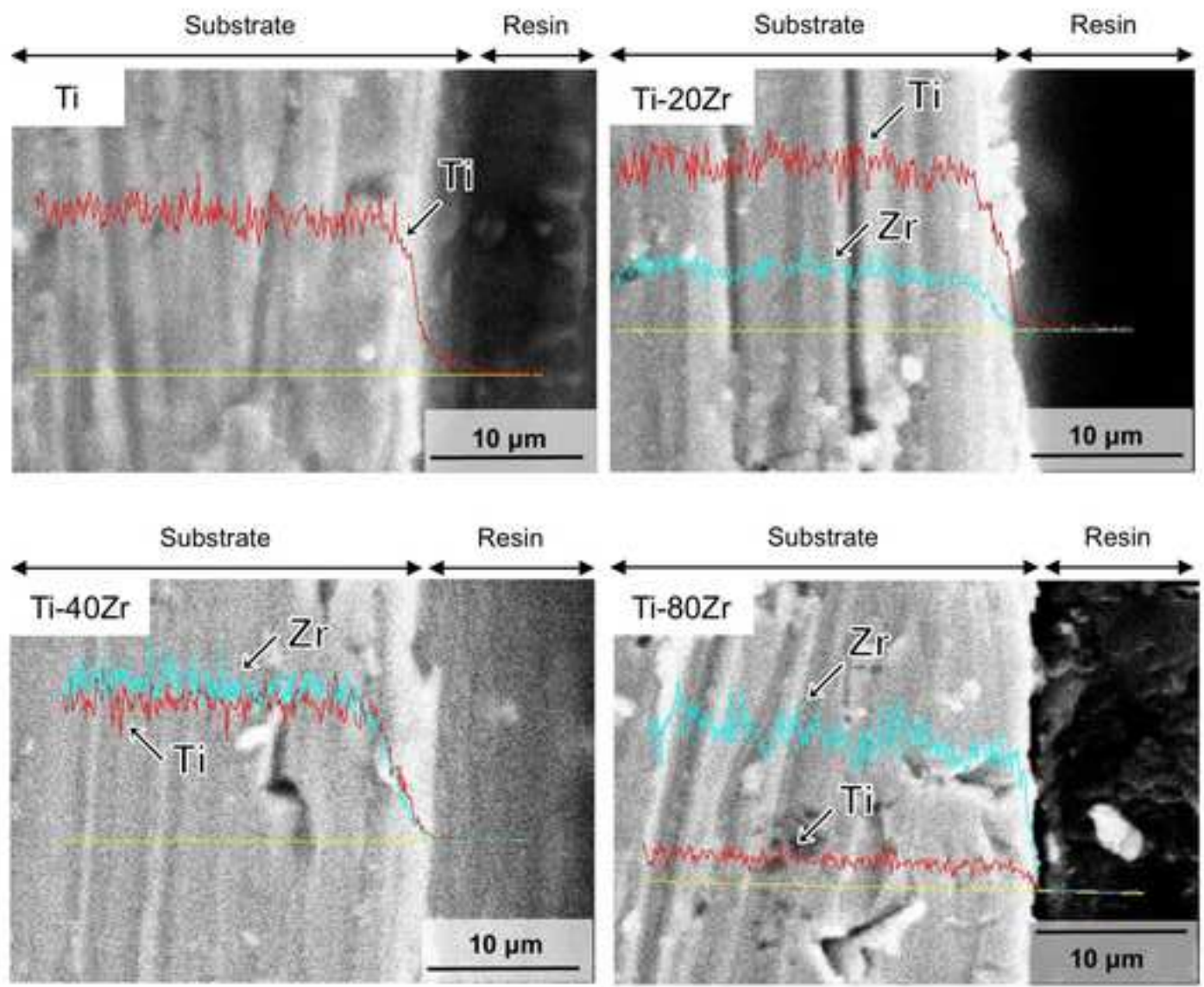


Fig. 6

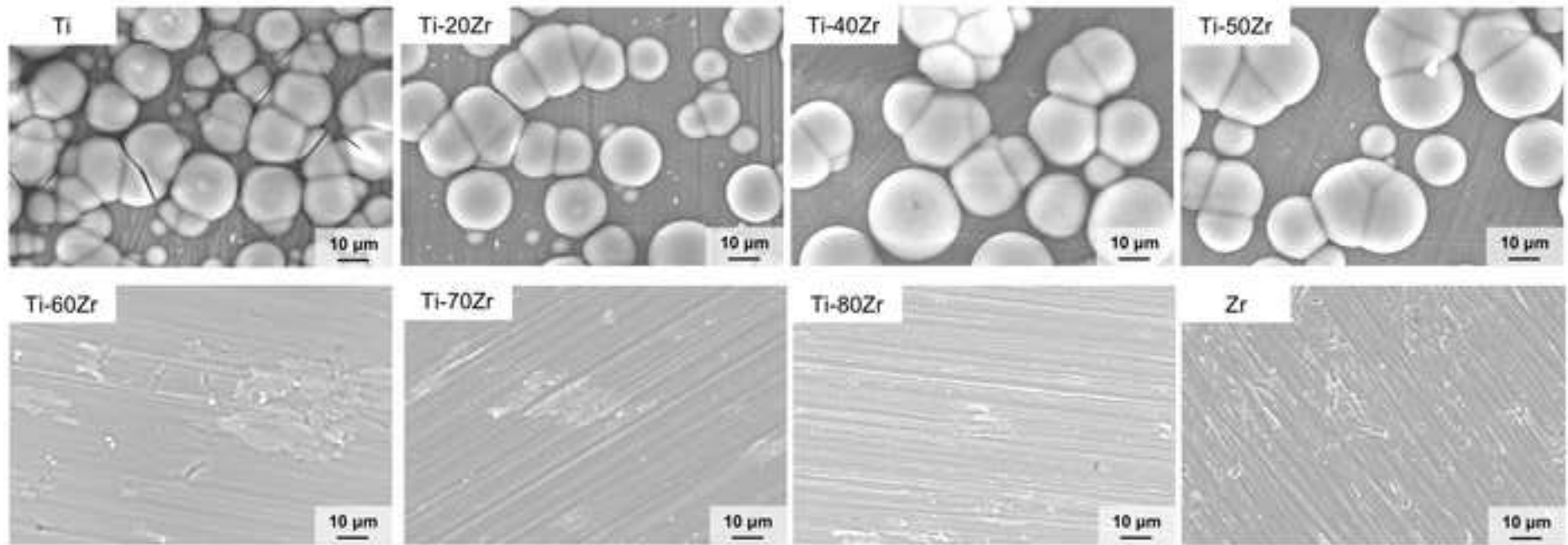


Fig. 7

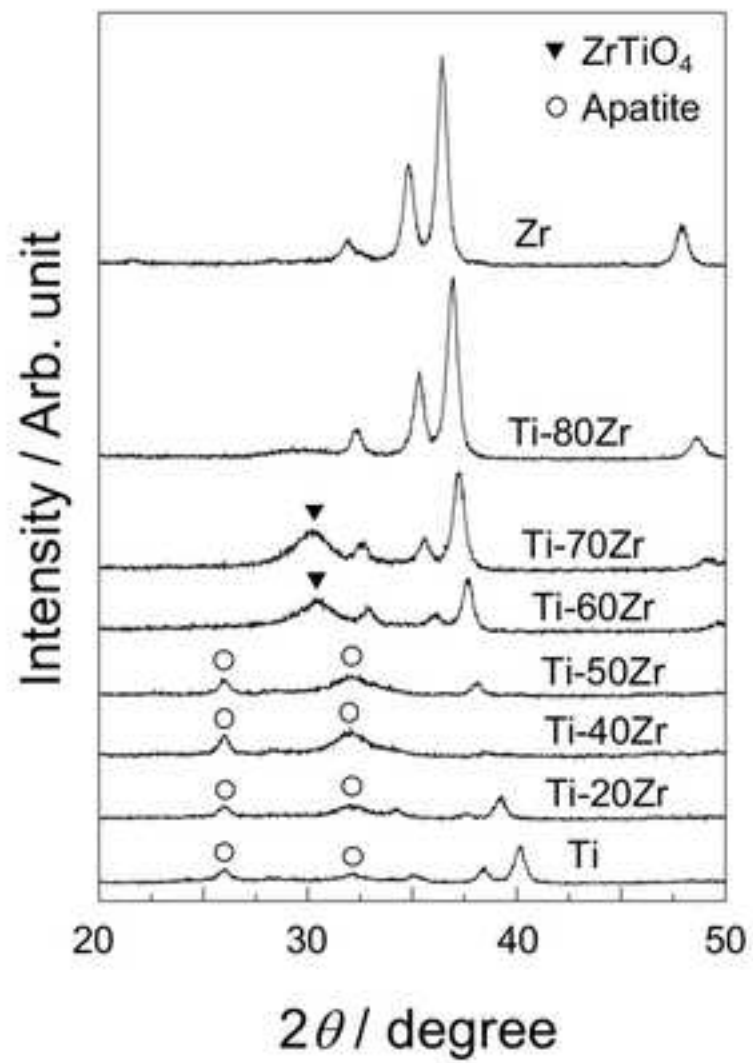


Fig. 8

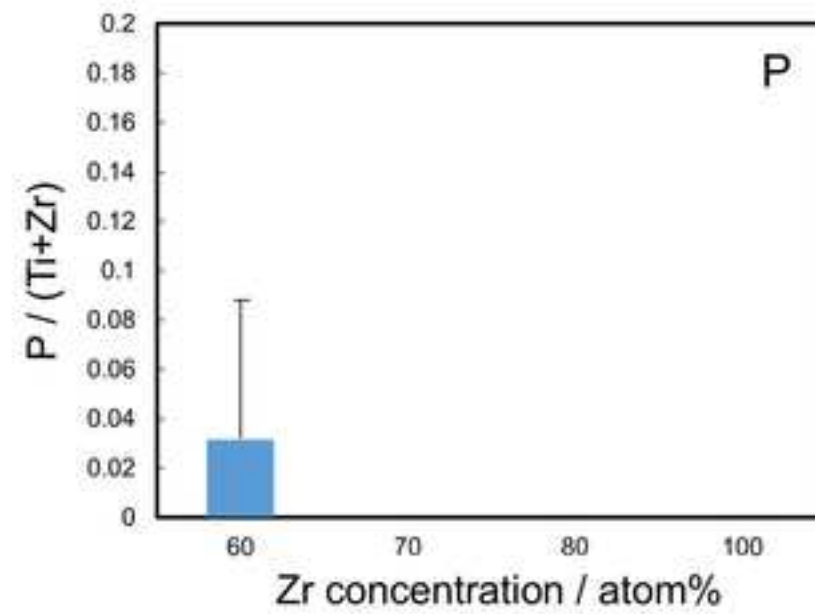
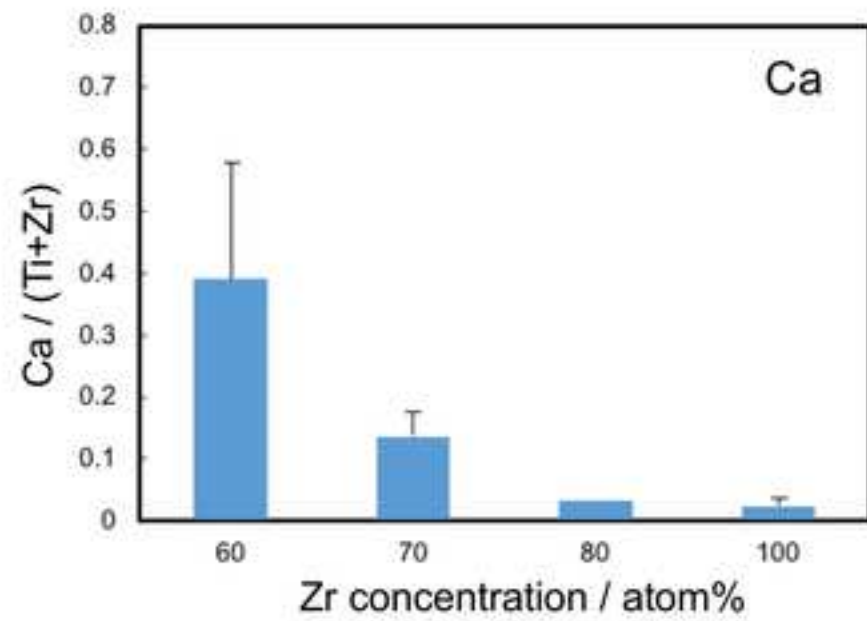


Fig. 9

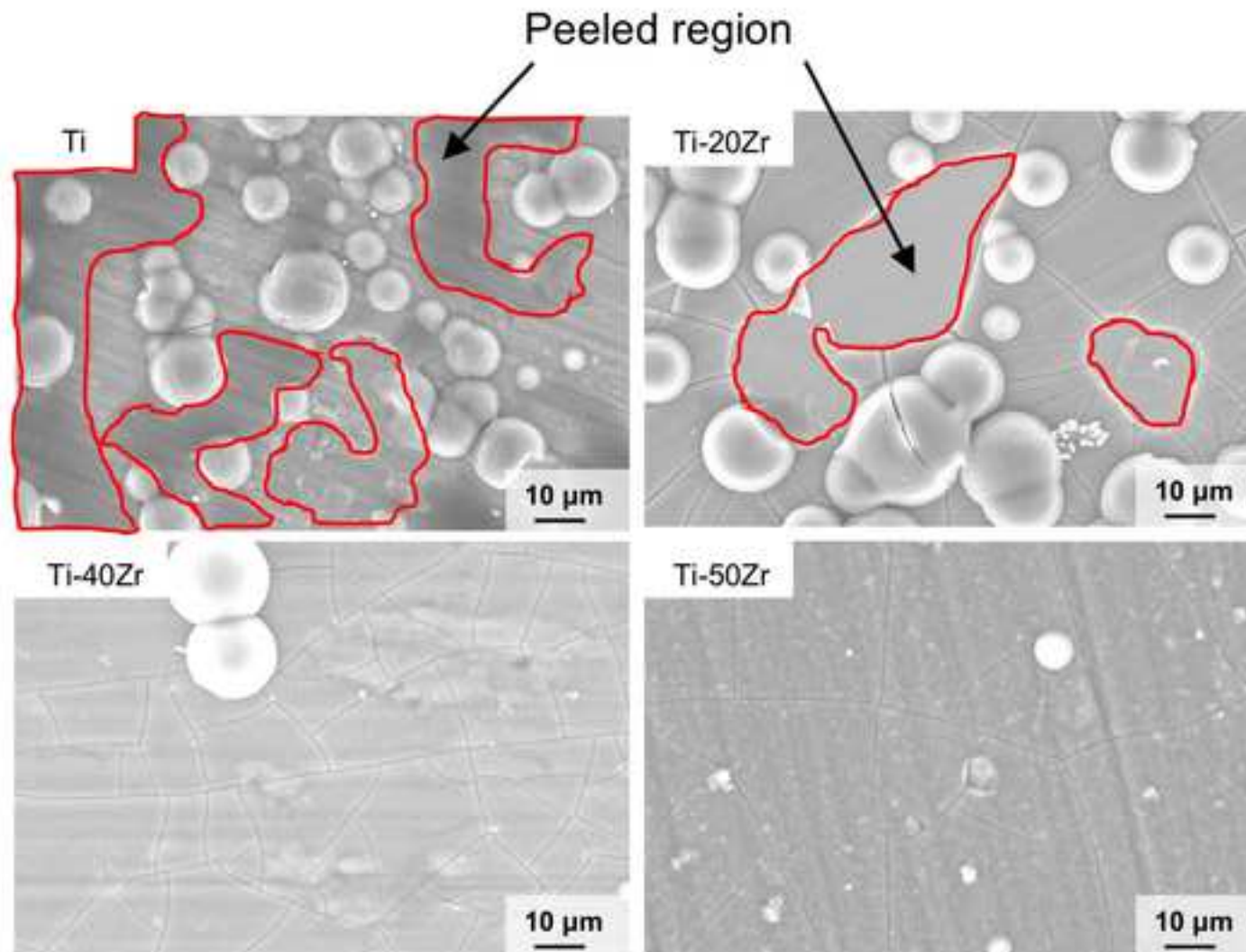


Fig. 10

